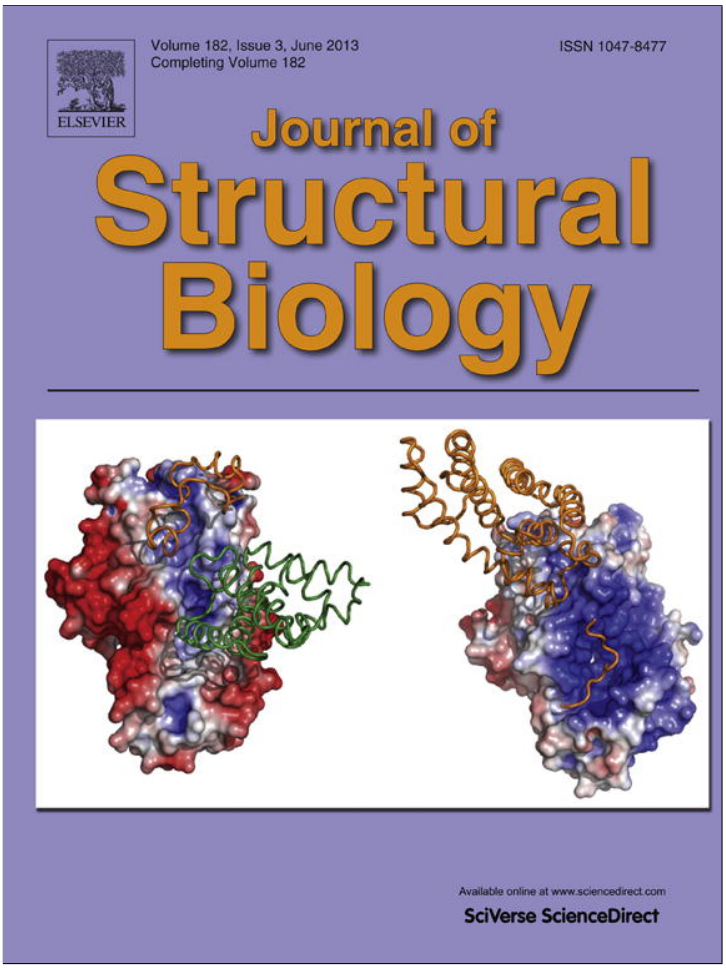

Journal of Structural Biology 182 (2013) 197–208

Contents lists available at SciVerse ScienceDirect

Journal of Structural Biology

journal homepage: www.elsevier.com/locate/yjsbi

The human ITPA polymorphic variant P32T is destabilized by the unpacking of the hydrophobic core

Peter D. Simone [a], Lucas R. Struble [b], Admir Kellezi [a], Carrie A. Brown [c], Corinn E. Grabow [a], Irine Khutsishvili [d], Luis A. Marky [a,b,d], Youri I. Pavlov [a,b,e,f], Gloria E.O. Borgstahl [a,b,d,*]

[a] The Eppley Institute for Research in Cancer and Allied Diseases, University of Nebraska Medical Center, 987696 Nebraska Medical Center, Omaha, NE 68198-7696, USA
[b] Department of Biochemistry and Molecular Biology, University of Nebraska Medical Center, Omaha, NE 68198, USA
[c] Department of Chemistry, Wayne State College, Wayne, NE 68787, USA
[d] Department of Pharmaceutical Sciences, College of Pharmacy, University of Nebraska Medical Center, Omaha, NE 68198-6025, USA
[e] Department of Pathology and Microbiology, University of Nebraska Medical Center, Omaha, NE 68198, USA
[f] Department of Genetics, St-Petersburg University, St-Petersburg 199034, Russia

ARTICLE INFO

Article history:
Received 20 June 2012
Received in revised form 11 March 2013
Accepted 13 March 2013
Available online 23 March 2013

Keywords:
Inosine triphosphate pyrophosphatase,
Nucleotide pool
X-ray crystallography
Protein stability
Hydrophobic surfaces
Genomic instability

ABSTRACT

Inosine triphosphate pyrophosphatase (ITPA), a key enzyme involved in maintaining the purity of cellular nucleoside triphosphate pools, specifically recognizes inosine triphosphate and xanthosine triphosphate (including the deoxyribose forms) and detoxifies them by catalyzing the hydrolysis of a phosphoanhydride bond, releasing pyrophosphate. This prevents their inappropriate use as substrates in enzymatic reactions utilizing (d)ATP or (d)GTP. A human genetic polymorphism leads to the substitution of Thr for Pro32 (P32T) and causes ITPA deficiency in erythrocytes, with heterozygotes having on average 22.5% residual activity, and homozygotes having undetectable activity. This polymorphism has been implicated in modulating patients' response to mercaptopurines and ribavirin. Human fibroblasts containing this variant have elevated genomic instability upon treatment with base analogs. We find that the wild-type and P32T forms are dimeric in solution and in the crystal structure. This abolishes the previous speculation that the P32T change disrupts dimerization as a mechanism of inactivation. The only difference in structure from the wild-type protein is that the area surrounding Thr32 is disrupted. Phe31 is flipped from the hydrophobic core out into the solvent, leaving a hole in the hydrophobic core of the protein which likely accounts for the reduced thermal stability of P32T ITPA and ultimately leads to its susceptibility to degradation in human cells. Circular dichroism and thermal denaturation studies confirm these structural results. We propose that the dimer of P32T variant subunit with wild-type subunit is degraded in cells similarly to the P32T homodimer explaining the level of loss of ITPA activity in heterozygotes.

1. Introduction

Maintenance of the quality of the nucleotide pool is crucial for numerous cellular processes, from DNA and RNA synthesis to the myriad reactions requiring ATP or GTP. One of the enzymes cleansing the nucleotide pool is inosine triphosphate pyrophosphatase (ITPA), a pyrophosphohydrolase, which acts on noncanonical purines, such as inosine triphosphate (ITP) and xanthosine triphosphate (XTP) (Lin et al., 2001). This prevents contamination of the nucleotide triphosphate pool which could lead to the incorporation of abnormal nucleotides into DNA and RNA (Pang et al., 2012) or the misuse of ITP/XTP by enzymes utilizing ATP/GTP (Behmanesh et al., 2009). Underscoring the importance of ITPA, more than half of *Itpa* knockout mice die before birth, and those that do survive display growth retardation, heart abnormalities, ataxia, and abnormal breathing and die within two weeks (Behmanesh et al., 2009). Furthermore, cells from *Itpa* knockout mice had elevated levels of inosine in the RNA and DNA and had more chromosomal abnormalities than wild-type cells (Abolhassani et al., 2010). This clearly demonstrates that the accumulation of non-canonical nucleotides interferes with normal cellular processes and can ultimately have dire consequences.

Abbreviations: ATP, adenosine triphosphate; βME, β-mercaptoethanol; CT, C-terminus; GTP, guanosine triphosphate; HAP, 6-hydroxylaminopurine; HSP, heat shock protein; ITP, inosine triphosphate; ITPA, inosine triphosphate pyrophosphatase; NT, N-terminus; NUDT16, nudix-type motif 16 protein; PEG, polyethylene glycol; RMS, root mean square; T_M, melting temperature; TPMT, thiopurine *S*-methyltransferase; XTP, xanthosine triphosphate.

* Corresponding author. Fax: +1 402 559 3739.
E-mail address: gborgstahl@unmc.edu (G.E.O. Borgstahl).

1047-8477/$ - see front matter © 2013 Elsevier Inc. All rights reserved.
http://dx.doi.org/10.1016/j.jsb.2013.03.007

ITPA is a homodimeric globular protein consisting of a long central β-sheet forming the floor of the active site, flanked by two mainly α-helical lobes (Porta et al., 2006; Stenmark et al., 2007). Upon substrate binding, these lobes close by approximately 25°. The nucleotide base is clamped in place by the ring structures of Phe149 and Trp151. Residues Lys172, His177, and Arg178 are within hydrogen bonding distance of the 6-keto oxygen of ITP. The amino group in this position on ATP could not be accommodated, explaining the ability of ITPA to discriminate between ITP and ATP. The low resolution of the ITP-bound structure does not permit a definitive reaction mechanism to be determined, but a water molecule coordinated by either Asn16 or Asp72 would be positioned for attack on the α-β phosphoanhydride bond.

In humans, several polymorphisms have been identified in the *ITPA* gene which result in varying degrees of ITPA deficiency. A 94C>A polymorphism, encoding for a protein with a proline to threonine substitution at amino acid 32 (P32T), causes ITPA deficiency (Cao and Hegele, 2002; Sumi et al., 2002). The frequency of this allele is highest in Asian populations, at 11–19% (Marsh et al., 2004). Individuals heterozygous for this mutation have 22.5% enzymatic activity in erythrocytes, compared to individuals with wild-type ITPA; homozygotes have no activity. Additional polymorphisms causing ITPA deficiency have been identified (summarized in (Bierau et al., 2007)), mainly in intron 2, but the P32T mutation leads to the most severe reduction in activity.

No overt phenotype has been associated with the polymorphisms causing ITPA deficiency. One explanation for the apparent contradiction between these observations and the results seen in knockout mice is that the P32T mutation does not completely abolish the function of the enzyme. In fact, the P32T mutant has been shown to have *in vitro* activity comparable to wild-type (Herting et al., 2010; Stepchenkova et al., 2009). In other cells besides erythrocytes, partial loss of activity could be compensated by higher levels of ITPA, thus preventing the phenotype seen in mice. This is supported by a demonstration that although the variation in activity seen in the erythrocytes of a random population correlates with the activity in granulocytes, lymphocytes, and platelets, the overall activity in these cells was much higher than in erythrocytes, which had the lowest activity of the cell types examined (Verhoef et al., 1980). Additionally, the expression of *ITPA* is known to vary among tissues, with the heart having one of the highest levels of expression (Lin et al., 2001). Another possibility is that an additional enzyme has parallel functions with ITPA; Abolhassani and coworkers suggest NUDT16, an inosine diphosphatase, as a candidate (Abolhassani et al., 2010). Hence, unlike knockout mice, human ITPA deficiency from the 94C>A polymorphism is likely not a complete deficiency even in homozygotes.

ITPA deficiency has been found to play a role in the negative response of patients to several drugs. Marinaki and coworkers were the first to discover an association between the 94C>A *ITPA* polymorphism and an increased occurrence of adverse reactions to azathioprine used in the treatment of inflammatory bowel disease (Marinaki et al., 2004). Azathioprine and other mercaptopurine drugs are also used in the treatment of leukemia and autoimmune disorders and are well known to produce negative side-effects such as rash, myelotoxicity, pancreatitis, and hepatoxicity in some patients. Another enzyme, thiopurine *S*-methyltransferase (TPMT) also functions in mercaptopurine metabolism and its deficiency due to polymorphism leads to hematopoietic toxicity (Krynetski and Evans, 1998; Relling et al., 1999). Stocco and coworkers have shown that the P32T form of ITPA is associated with febrile neutropenia in acute lymphoblastic leukemia patients treated with mercaptopurines when the dose was adjusted based on *TPMT* genotype, and they suggest that inconsistencies in previous studies may be due to a failure to individualize mercaptopurine doses based on *TPMT* genotype (Stocco et al., 2009). Furthermore, a study examining the association between ITPA activity, rather than specific genotypes, and azathioprine toxicity in chronic inflammatory bowel disease found elevated levels of adverse reactions in patients with low ITPA activity. This suggests that the disagreement between previous studies may be due to including patients with other ITPA deficiency alleles in the control group and/or to variable degrees of ITPA deficiency in a given genotype (Shipkova et al., 2011). Hence, ITPA appears to be an important player in mercaptopurine metabolism and toxicity.

On the other hand, beneficial effects of the P32T polymorphism have been noted in certain patients. This polymorphism was associated with a better response to low-dose azathioprine in the treatment of systemic lupus erythematosus (Okada et al., 2009). Most recently, ITPA deficiency was found to protect against hemolytic anemia in hepatitis C patients treated with ribavirin (Fellay et al., 2010; Ochi et al., 2010; Sakamoto et al., 2010; Thompson et al., 2010). Together, these data show that ITPA deficiency can have both beneficial and deleterious effects and its pharmacogenetic profile must be considered when a patient's treatment is planned.

P32T ITPA has also been shown to contribute to genomic instability (Waisertreiger et al., 2010). When human fibroblasts homozygous for the 94C>A ITPA polymorphism were treated with a non-canonical purine analog, an increased amount of DNA breaks was found relative to wild-type cells. A similar result was seen in cells in which *ITPA* was knocked down by shRNA (Menezes et al., 2012). This suggests that base analogs accumulate in cells with low ITPA activity and can be inserted into DNA, where they are recognized by an endonuclease, creating a single-strand break, or a glycosylase, creating an abasic site which also ultimately leads to a single strand-break. These single-strand breaks, if not repaired before DNA replication, can lead to double-strand breaks and genomic instability (Friedberg et al., 2006).

2. Materials and methods

2.1. Protein expression, spot activity assay and purification

The pET15b-ITPA vector and its derivatives were used for spot tests and protein purification from bacteria. Creation of the wild-type and P32T ITPA expression vectors has been described (Porta et al., 2006; Stepchenkova et al., 2009). To create the *ITPA* allele encoding for the replacement of proline with alanine at codon 32 in ITPA, site directed mutagenesis on the pET15b-ITPA was performed using the following primer set: 5′ GGAGATAAGTTTGCATGCACTTTGG and 5′ CCAAAGTGCATGCAAACTTATCTCC using Quick Change kit from Stratagene. Sequencing to verify the change was done with primers ITPA_sN (5′ TCATTGGTGGGGAAGAAGATC) and ITPA-sC (5′ AAGCTGCCAAACTGCCAAA).

The spot test assay for protection of *E. coli* from the base analog 6-hydroxylaminopurine (HAP) was performed on Vogel-Bonner minimal media (Vogel and Bonner, 1956) as previously described (Kozmin et al., 2008; Stepchenkova et al., 2009). The only difference was the use of NEB195 *E. coli* cells BL21(DE3) with a deletion of *rdgB* encoding for bacterial ITPase (Burgis and Cunningham, 2007) or transformation with pET15b-ITPA variants. This strain was kindly provided by Dr. R. Cunningham and Dr. N. Burgis.

Wild-type, P32T and P32A ITPA were expressed and purified as described before (Porta et al., 2006; Stepchenkova et al., 2009) with the following modifications. Following induction with 1 mM isopropyl β-D-1-thiogalactopyranoside, the bacterial cultures were grown overnight at 18 °C. Bacteria pellets were resuspended in 20 mM bicine pH 8.5, 40 mM imidazole, and 2 mM βME. After initial purification by Ni chromatography, the His-tag was cleaved with thrombin, and the thrombin removed with benzamidine resin. Then batch chromatography with Ni–NTA agarose (Qiagen)

was performed to remove the cleaved His-tag followed by anion-exchange chromatography with a Q FF resin (GE Healthcare) using an elution gradient of 0–500 mM NaCl over 50 column volumes. The proteins were dialyzed against 2 L of the indicated buffers. Protein concentrations were determined by measuring the absorption at 280 nm with a NanoDrop® ND-1000 Spectrophotometer blanked with dialysis buffer, and using a calculated molar extinction coefficient of 19,940 M^{-1} cm^{-1} and a molecular weight of 21.73 kDa as determined by ExPASy ProtParam (web.expasy.org/protparam/).

2.2. Crystallization and data collection

P32T ITPA was concentrated to approximately 24 mg/mL in 20 mM bicine, 150 mM NaCl, and 2 mM βME at pH 8.5 using Amicon Ultra 3000 MWCO centrifugal concentrators (Millipore) and mixed 1:1.5 on a glass coverslip with a reservoir solution containing 0.1 M bis-tris, 24.4% w/v PEG 3350, and 10 mM βME at pH 6.7. The coverslip was inverted and sealed over the reservoir. Crystals grew within one day at room temperature. The crystal was mounted on a MicroMount loop (MiTeGen) and dragged through a cryoprotectant solution with the same composition as the reservoir solution except for 30% w/v PEG 3350.

X-ray diffraction data were collected at 100 K with a Rigaku FR-E Cu *Kα* rotating-anode generator operating at 45 kV and 45 mA and equipped with an R-AXIS IV++ detector and Xstream 2000 low-temperature system. A full native data set to 2.07 Å was collected as 196 images with 0.5° oscillation at a crystal-to-detector distance of 150 mm with 8 min exposure times. The data were processed with CrystalClear (Rigaku). Data collection statistics and refinement parameters are shown in Table 1.

2.3. Structure determination and refinement

Molecular replacement was performed with PHENIX (Adams et al., 2010) using as a search model wild-type ITPA (PDB code 2I5D (Porta et al., 2006)) with solvent and alternate conformations removed and Pro32 mutated to alanine. The structure was improved by rounds of reciprocal space and real space refinement using PHENIX and Coot (Emsley et al., 2010), respectively. To eliminate model bias, omit maps were made with MOLEMAN2 (Kleywegt, 1997) and PHENIX. Residues Gly(-2), Ser(-1), His0, Met1, Ala2, Leu192, Ala193, and Ala194 were deleted due to lack of electron density. Residues Ser4, Glu44, Ile52, and Gln127 were modeled with dual conformations.

Table 1
Diffraction data and refinement statistics. The X-ray data were processed using CrystalClear 2.0 (Rigaku Corporation). Values in parentheses are for the highest resolution bin.

PDB code	4F95
Space group	$P2_12_12$
Unit-cell parameters (Å)	a = 31.02, b = 104.42, c = 50.36
Z (No. of molecules per ASU)	1
V_M (Å^3 Da^{-1})	1.88
Solvent content[a] (%)	34.46
Resolution range (Å)	29.74–2.07 (2.14–2.07)
No. of observed/unique reflections	38543/10531
Completeness (%)	100.0 (100.0)
Multiplicity	3.66 (3.71)
R_{sym}[b] (%)	5.7 (47.8)
$I/\sigma(I)$	9.9 (2.1)
R_{work} (%)	23.4
R_{free} (%)[c]	30.8
No. of protein atoms modeled/No. possible	1477/1529
No. of water molecules	68
R.m.s.d. bonds (Å)	0.009
R.m.s.d. angles (°)	1.252
Ramachandran analysis (%)	
Residues in most favorable region	98.4
Residues in allowed regions	1.1
Residues in disallowed regions	0.5
Average B (Å^2)	
Protein	49.18
Water	45.01

[a] Solvent content was calculated based on the Matthews coefficient (Matthews, 1968): 1–1.23/V_M.
[b] $R_{sym} = \Sigma_{hkl} |I_{hkl} - \langle I_{hkl} \rangle| / \Sigma_{hkl} I_{hkl}$.
[c] The R_{free} test set size was 5% (Brunger, 1993).

2.4. Dynamic light scattering

Dynamic light scattering measurements were taken on wild-type and P32T ITPA using a DynaPro MS/X instrument (Protein Solutions) with ASTRA® V software (Wyatt). Samples were filtered through a 0.02 μm filter using the Protein Solutions MicroFilter system into a 1.50 mm quartz cuvette (Wyatt). Measurements were taken at 22 °C and 20 acquisitions were taken per sample with a baseline limit of 0.1.

2.5. Circular dichroism

Circular dichroism data were collected on an Aviv Stopped Flow Circular Dichroism Spectrophotometer Model 202SF (Aviv Biomedical, Inc.) using a 0.2 cm quartz cuvette (Hellma). The proteins were dialyzed into 2 mM bicine, pH 7.8, and 0.5 mM βME and then proteins were diluted to the desired concentration with 1X PBS. The protein concentration where the absorbance at 222 nm and 280 nm were equal to 1.0 was used for wavelength scans (0.085 and 1.30 mg/mL, respectively). Three scans were taken at 25 °C for the buffer, wild-type, and P32T ITPA from 200 to 270 nm and 260–320 nm, sampling every 1 nm with an averaging time of 5 s. The three scans were averaged, the buffer data were subtracted, and then the data were converted to mean residue ellipticity. The curves were smoothed with a Savitzky-Golay filter (Savitzky and Golay, 1964) using the Microsoft Excel add-in MacroBundle (www.bowdoin.edu/~rdelevie/excellaneous/). Then the baseline at 270 or 320 nm was subtracted from each spectrum.

2.6. Fluorescence spectroscopy

Protein samples were prepared the same way as for circular dichroism and were diluted to 4.6 μM. The fluorescence measurements were obtained using an AVIV Model-ATP105 spectrofluorometer (Lakewood, NJ), equipped with a Peltier system for temperature control. The fluorescence emission spectrum of each protein was obtained from 300 nm to 500 nm at 20 °C, using an excitation wavelength of 290 nm. The emission and excitation slits were set at 2.5 nm. This allowed us to select the wavelength of maximum fluorescence emission of tryptophan, 345 nm, for the temperature-induced denaturation studies. Fluorescence melting curves were obtained by measuring the intensity of fluorescence at 345 nm from 25 °C to 95 °C using a heating rate of 1 °C/min. In order to compare the shape of the melting curves of these proteins, all curves were normalized to zero fluorescence intensity at high temperatures, allowing us to determine T_Ms using a procedure described earlier (Marky and Breslauer, 1987).

3. Results

3.1. Structure determination of P32T ITPA

In order to determine in atomic detail how the P32T change affects the enzymatic activity in cells, we solved the protein structure of P32T ITPA by X-ray crystallography. Native crystal conditions did not yield crystals. For crystal growth, it was

essential that the concentration of buffer components was optimized using dynamic light scattering methods (Borgstahl, 2007; Habel et al., 2001). Increasing the NaCl concentration to 100–150 mM gave a percent polydispersity of 9.6% which indicates a high likelihood of crystallizability. P32T ITPA had a hydrodynamic radius of 3.0 nm consistent with a dimer and identical to wild-type (data not shown). Orthorhombic crystals were grown and diffraction data were collected. Since one structure of wild-type ITPA (PDB code 2CAR (Stenmark et al., 2007)) came from a pseudo-merohedrally twinned crystal, we analyzed our data for merohedral twinning using both the Merohedral Crystal Twinning Server (Yeates, 1997) and the Merohedral Twin Detector: Padilla-Yeates Algorithm (Padilla and Yeates, 2003), neither of which indicated twinning (data not shown). Both wild-type and P32T ITPA crystallized in the orthorhombic space group $P2_12_12$. Data collection and refinement statistics are summarized in Table 1.

Overall, the structure of P32T ITPA was very similar to wild-type ITPA. However, the P32T ITPA crystal structure showed very weak electron density in the region around Thr32 (Fig. 1A and B), indicating a high degree of disorder in this area of the protein. Omit maps calculated with F_o-F_c coefficients revealed electron density that allowed the overall position of the residues to be ascertained (Fig. 1C). It should be cautioned, though, that the lack of well-defined electron density for these residues makes definitive placement not possible, and in fact the residues probably exist in numerous conformations. For the remainder of the protein, however, the residues were well ordered, with clear $2F_o-F_c$ electron density (Fig. 1D).

Wild-type and P32T ITPA crystallized in isomorphous space groups which allowed the calculation of difference maps between the two crystals. When a F_o-F_o difference map ($F_{P32T}-F_{wild\text{-}type}$) was calculated, several structural changes were immediately apparent in the vicinity of Thr32 (Fig. 2). The loop containing the P32T change has clearly moved as it appears in negative electron density (red) in the wild-type structure, and there is corresponding positive density (green) nearby where Thr32 was modeled (Fig. 2A). The C-terminus of wild-type ITPA is surrounded by negative density, but there is no positive density for P32T ITPA, indicating that the C-terminus of the mutant is disordered (Fig. 2B). The side chain of Phe189 of P32T has shifted position toward the location of Phe31 in the wild-type structure (Fig. 2C). Overall, the conclusions drawn from the $F_{P32T}-F_{wild\text{-}type}$ maps (Fig. 2) agree with the omit maps (Fig. 1C).

P32T ITPA was crystallized without nucleotide and is in the open conformation. When the structures of wild-type ITPA in the open state and P32T ITPA are superimposed, the majority of the structures overlap well (Fig. 3A). In Fig. 3A, the nucleotide position from PDBID 2J4E was overlaid as a point of reference (Stenmark et al., 2007). Of note, there are no major changes to the active site cleft, which agrees with the observation that P32T ITPA maintains wild-type levels of enzymatic activity (Stepchenkova et al., 2009). On the other hand, several structural differences can be seen in the vicinity of Thr32 (Fig. 3B). The position of the backbone for the residues near Thr32 is shifted, causing Phe31 and Thr32 to be flipped out into the solvent. The side chain of Phe189 moves towards the space occupied by Phe31 in the wild-type structure, again consistent with the $F_{P32T}-F_{wild\text{-}type}$ map. The remainder of the C-terminus continues along a different trajectory, although the final three residues (Leu192, Ala193 and Ala194) were unable to be modeled due to lack of electron density. The N-terminus also appears to no longer form a short α-helix, and as with the C-terminus, the first several residues were unable to be modeled (Met1 and Ala2 and an artificial Gly-Ser-His sequence from the His-tag left after thrombin cleavage). Alignment of the Cα atoms for all residues with wild-type ITPA (PDB code 2I5D) using *LSQKAB* (Kabsch, 1976) in *CCP4i* (Collaborative Computational Project, 1994; Potterton et al., 2003) gives an RMS displacement of 1.04 Å, with the greatest differences occurring at the termini and near Thr32. Eliminating the termini and 29–34 loop from the alignment reduces the RMS displacement to 0.35 Å. Thus the majority of the secondary structure is the same between wild-type and P32T ITPA.

By further comparing the P32T mutant to the wild-type protein, we found that the average *B*-factor for the protein atoms is over 28 Å^2 greater for the mutant protein. The *B*-factor from the Wilson plot is similarly higher for P32T (44.9 Å^2) vs. wild-type ITPA (20.8 Å^2). For all atoms, the refined *B*-factors in the P32T structure are greater than for the corresponding atoms in wild-type ITPA, and the three largest differences in *B*-factor occur at the N-terminus, the area around Thr32, and the C-terminus, with the area around Thr32 having the largest difference (ΔB-factor = 73.93 for residues Lys30–Thr34). This is indicative of an overall greater disorder in the P32T mutant, with the region around Thr32, including the N- and C-termini, having the greatest disorder and/or flexibility.

The P32T ITPA crystal structure revealed a dimer, consistent with our light scattering studies showing that P32T ITPA exists as a homodimer in solution (Stepchenkova et al., 2009). It was proposed that the level of activity seen in heterozygotes might be due to impaired dimer formation (Stenmark et al., 2007; Sumi et al., 2002). The structure of the dimer interface for P32T ITPA is identical to the wild-type protein (see Fig. S1A, in supplement) and approximately 1100 Å^2 of surface area is buried in the dimer interface, as determined by *PISA* (Krissinel and Henrick, 2007). The dimer interface is extensive, involving numerous hydrophobic interactions and multiple hydrogen bonds. The data from the crystal structure and dynamic and static light scattering conclusively show that the reduction in activity seen in patients with P32T ITPA cannot be due to a dimerization impairment. In fact, since the dimeric interface is not affected by the P32T change, it is likely that homodimers as well as heterodimers of ITPA are present in patients heterozygous for the P32T allele. A model to explain the loss of activity consistent with the current data will be presented in the Discussion section.

3.2. Circular dichroism studies support the P32T crystal structure

Next, we analyzed the differences in secondary structure by circular dichroism (CD). The secondary structures of wild-type and P32T ITPA are similar and accordingly the CD spectra overlap (Fig. 4A). There are some reproducible differences between 222 and 209 nm showing that the wild-type ITPA has more secondary structure than P32T ITPA. Estimates of secondary structure content were obtained with DichroWeb (Whitmore and Wallace, 2004) using the K2d algorithm (Andrade et al., 1993). Wild-type ITPA had 24% α-helix and 23% β-sheet. P32T ITPA had 19% α-helix and 24% β-sheet. So, the P32T amino acid change has some measurable effect on the α-helical content of the protein which supports the structural changes and disorder observed in the electron density maps for the Thr32 region and the N- and C-termini of P32T ITPA.

The CD spectra in the region 260–320 nm arise from the aromatic amino acids and provide a tertiary structure fingerprint (Kelly et al., 2005). The shape and magnitude of this region of the CD spectrum of a protein will depend on the number of each type of aromatic amino acids, their mobility, the nature of their environment and their spatial distribution in the protein. ITPA has 11 Phe, 6 Tyr and 2 Trp. The Phe and Tyr portions of the spectra (Fig. 4B) are reproducibly different, as predicted by the crystal structure comparison (see also Fig. S1B and S1C, in supplement). Differences in the Trp region of the spectra are minimal probably because all Trp are located far away from the mutation site. These data suggest that P32T ITPA is not able to correctly fold its tertiary structure and support the crystal structure.

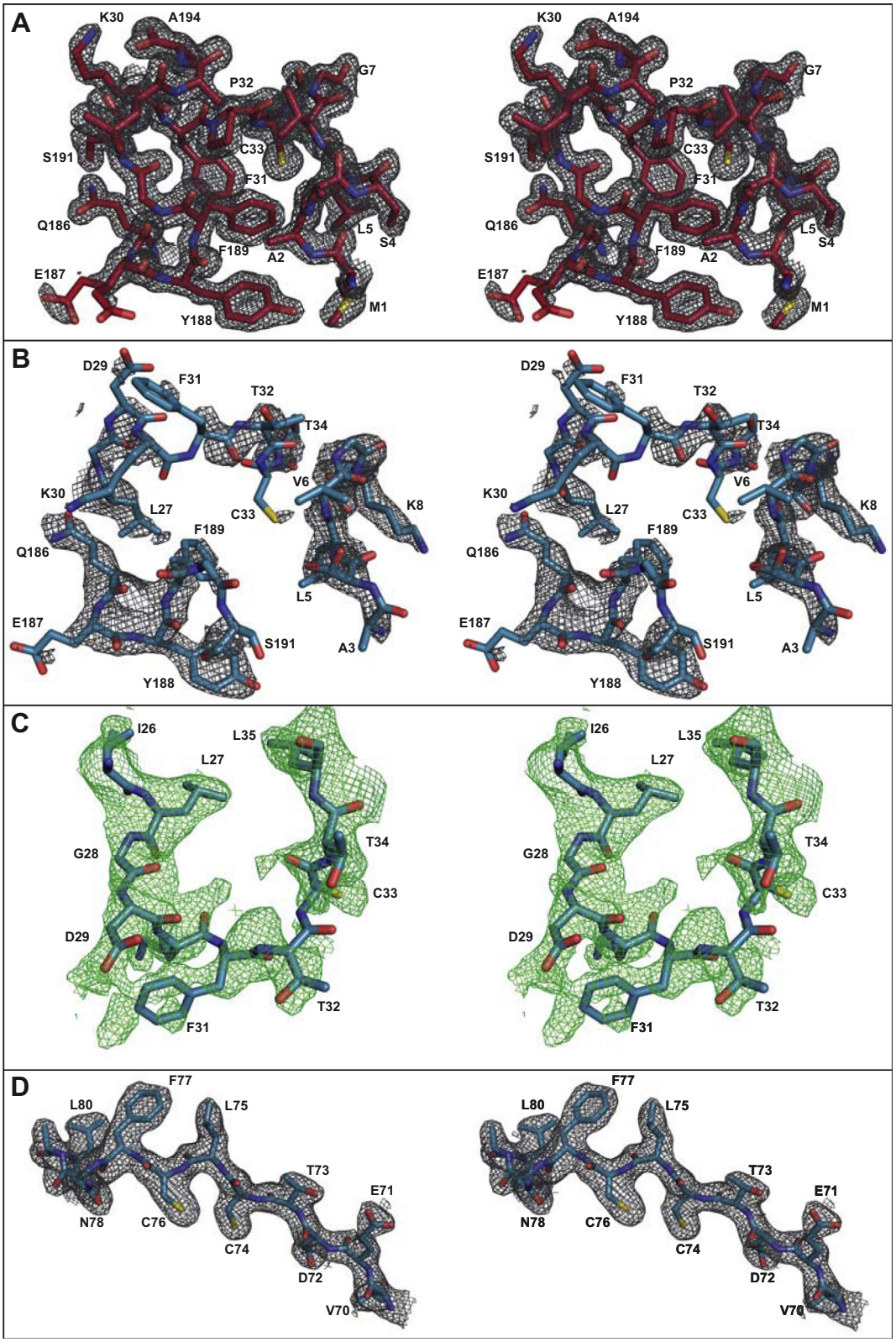

Fig.1. Representative electron density maps. (A) Wild-type ITPA (PDB code 2I5D (Porta et al., 2006)) shows clear, easily interpretable $2F_o–F_c$ electron density at 1.63 Å in the vicinity of P32 (σ = 1.0). (B) By contrast, P32T ITPA has poor or absent $2F_o–F_c$ electron density at 2.07 Å in this region, indicative of disorder (σ = 1.0). (C) $F_o–F_c$ omit maps reveal the positions of the residues lacking $2F_o–F_c$ electron density (σ = 1.5). (D) A representative area of P32T ITPA demonstrates that the majority of the protein was well ordered, with readily apparent $2F_o–F_c$ electron density (σ = 1.0). Wall-eyed stereo pairs were generated with *PyMOL* (Schrodinger, 2011).

3.3. P32T ITPA is less thermally stable than wild-type ITPA

We thought that we could monitor differences near the P32T mutation using Phe fluorescence, but the signal from ITPA was dominated by Trp fluorescence. The Trp are located in the heart of the dimer interface (Trp90) and in the active site (Trp151) (see Fig. S1B, in supplement). We had previously demonstrated that wild-type ITPA in 20 mM bicine (pH 8.5) and 50 mM NaCl at a

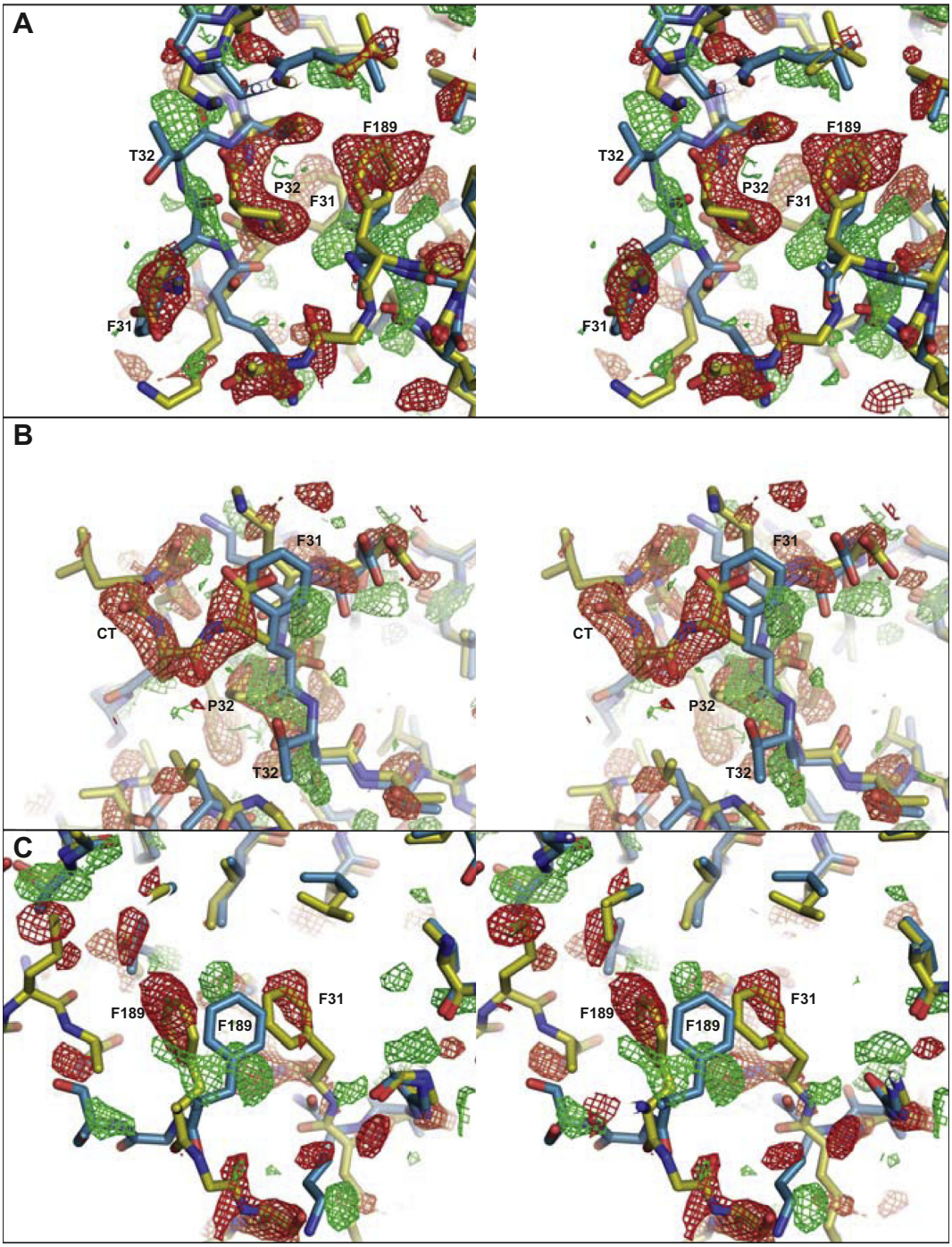

Fig.2. Difference F_{P32T}–$F_{wild\text{-}type}$ electron density maps. (A) A view of the Pro32 loop shows negative density (red) around the position in the wild-type protein (yellow), while the P32T mutant (blue) is located in positive density (green). (B) The C-terminus of wild-type ITPA is surrounded by negative density, but there is no corresponding positive density for the P32T mutant, indicating that it is disordered. Phe31 of P32T ITPA occupies the space where the C-terminus is in the wild-type protein. (C) Phe31 and Phe189 of wild-type ITPA are located in negative density. In the P32T mutant, Phe189 is shifted into positive density. Note that no density is present where atoms in the wild-type structure overlap with atoms in the mutant structure. Wall-eyed stereo pairs were generated with *PyMOL* (Schrodinger, 2011). (For interpretation of the references to color in this figure legend, the reader is referred to the web version of this article.)

protein concentration of 0.27 mg/mL (12 μM) had a melting temperature (T_M) of 56.7 °C using UV denaturation curves (Stepchenkova et al., 2009). P32T ITPA had a T_M that was 3.3 °C lower. Note these are similar buffer conditions to those used in wild-type ITPA crystallization. Trp fluorescence data (Fig. 4C) were reproducible but not reversible and gave a T_M of 61.3 °C for wild-type ITPA at 4.6 μM. This suggests that the phosphate buffered saline had an overall stabilizing effect on the protein fold. The P32T mutant T_M was 58.1 °C and the ΔT_M was 2.1 °C. Thus, the P32T ITPA is less thermally stable than wild-type ITPA in these buffer conditions as well.

3.4. Structural basis for decreased P32T ITPA stability

To understand how the P32T mutation causes these structural changes, first, a comparison of the backbone dihedral angles in

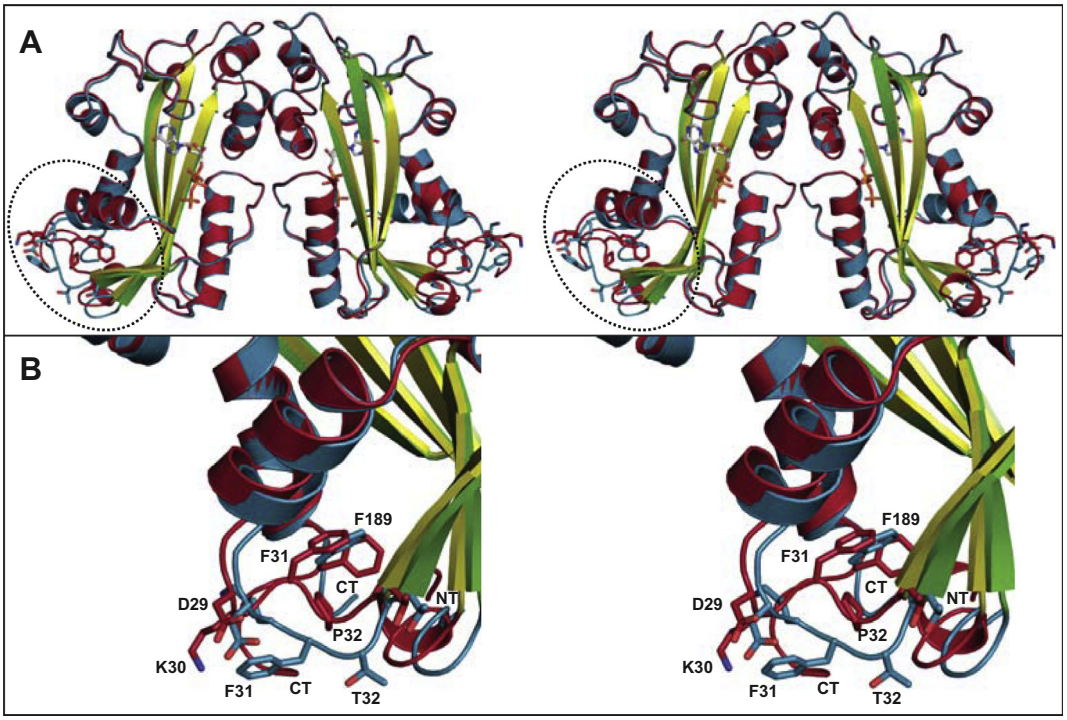

Fig.3. Structural differences between wild-type and P32T ITPA. (A) Wild-type ITPA is shown in red and yellow and P32T ITPA is shown in blue and green. The structures align well with the exception of the region around the P32T mutation, which includes the N- and C-termini. Notably, there are minimal changes to the active site cleft and the dimerization interface. (B) A zoomed in view of the area circled in (A) shows several major changes. The N- and C-termini have altered trajectories. The loop containing Thr32 has shifted towards the surface of the protein, with both Phe31 and Thr32 flipped out into the solvent. Phe189 has changed position to move closer to the space previously occupied by Phe31. Wall-eyed stereo pairs were generated with *PyMOL* (Schrodinger, 2011). (For interpretation of the references to color in this figure legend, the reader is referred to the web version of this article.)

the wild-type and mutant structures shows that the largest difference in the ϕ angle occurs for Phe31 and Thr32, while the largest difference in the ψ angle occurs at the N- and C-termini. The ring structure of proline restricts ϕ to a range of $-50°$ to $-100°$ (Lovell et al., 2003). In wild-type ITPA, Pro32 has a ϕ angle of $-88.0°$, but in the mutant this restriction is removed and Thr32 has a ϕ angle of $+76.8°$, a difference of nearly 180°. Second, modeling a threonine for Pro32 in wild-type ITPA shows that the polar hydroxyl group would be located in the hydrophobic pocket near Phe31 and Phe189 and/or clashes of greater than 1 Å would occur with neighboring residues (Val6 or Ala193 depending on the rotamer of threonine chosen), as determined by *MolProbity* (Chen et al., 2010; Davis et al., 2007) (Fig. 5). It is likely that these steric and electrostatic/hydrophobic effects, combined with the greater backbone torsional freedom, lead to the observed dramatic changes in protein structure.

To test this mechanism we created and purified a P32A ITPA mutant. This change is expected to relieve the restraints on the dihedral angles, but should not have steric clashes with atoms in the wild-type tertiary structure. The protection of *E. coli* from the base analog HAP was very similar for wild-type, P32T and P32A ITPA (results not shown), indicating that the enzymatic activity of P32A ITPA is normal. To see if the fold of P32A is similar in stability to wild-type or P32T we studied its melting curve by monitoring Trp fluorescence. The result lies in between the P32T and wild-type data and is most similar to the P32T data (Fig 4C). This test indicates that the main mechanism for the disorder of P32T is caused by the relief of restraints on the dihedral angles.

4. Discussion

Purified P32T ITPA has enzymatic activity similar to the wild-type enzyme, indicating that the loss of activity in erythrocytes *in vivo* is indirect (Herting et al., 2010; Stepchenkova et al., 2009). This begs the question of how the P32T substitution causes the observed lack of activity *in vivo*. The 94C>A polymorphism results in missplicing of exons 2 and 3 in 61% of the *ITPA* mRNA, accounting for some of the loss of activity, but this does not explain zero activity (Arenas et al., 2007).

With the structure of P32T ITPA in hand, we can understand how the amino acid change brings about the observed reduction in protein stability. First, the hydrophobic side chain of Phe31 is flipped from the hydrophobic core out into the solvent. This leads to a greater than 100 Å^2 increase in the solvent exposed surface area of Phe31 relative to wild-type (measured by *AREAIMOL* (Lee and Richards, 1971; Saff and Kuijlaars, 1997) in *CCP4i* (Collaborative Computational Project, 1994; Potterton et al., 2003)). As would be expected, solvent-exposed hydrophobic residues tend to be destabilizing in *in vitro* stability assays (Schwehm et al., 1998; Strub et al., 2004). This likely contributes to the reduced stability seen with P32T ITPA. At the same time, this movement of Phe31 leaves a cavity in the hydrophobic core of the protein, further destabilizing it (Fig. 6). The volume of the cavity is 887 Å^3, compared to only 159 Å^3 in the wild-type protein (as determined by *VOIDOO* (Kleywegt and Jones, 1994)). It was shown previously that creating a cavity in the hydrophobic core of bovine pancreatic RNase A decreased the stability of the enzyme (Kadonosono et al., 2003). Similarly, wild-type ITPA has a well packed hydrophobic core that is disrupted by the P32T mutation.

4.1. Potential consequences of unpacking the hydrophobic core

The less stable P32T ITPA protein fold could result in ITP accumulation through three pathways (Fig. 7A). First, the solvent-exposed phenyalanine could lead to P32T ITPA being sequestered by chaperones. The HSP70 family of proteins is known to bind to

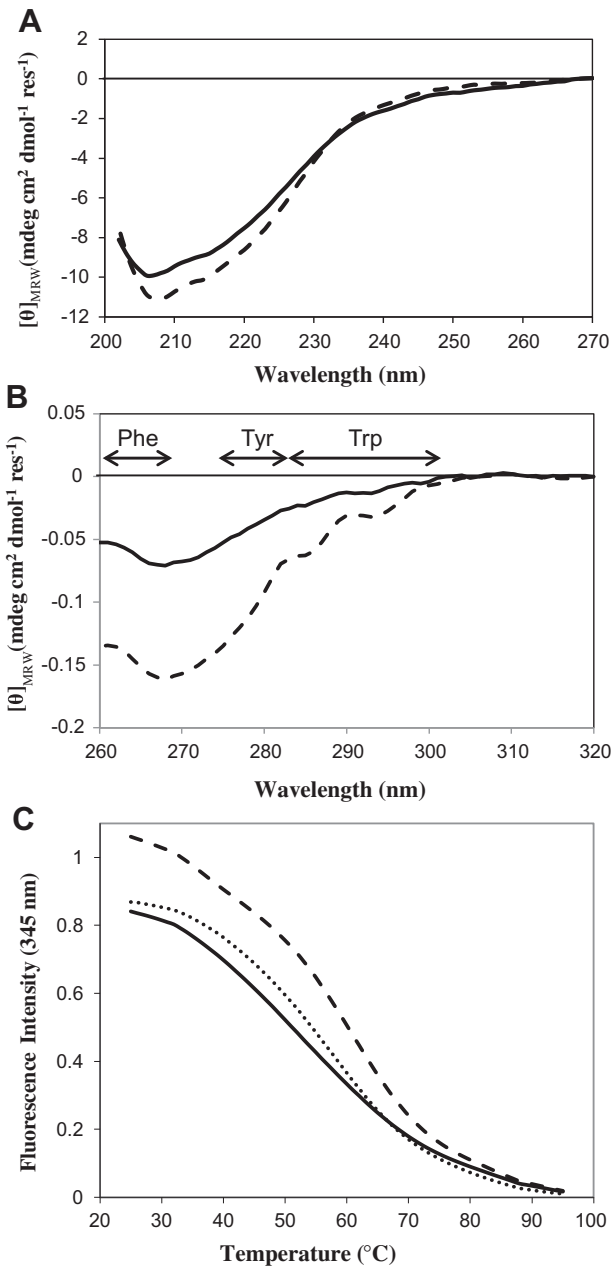

Fig.4. Comparison of secondary and tertiary structure and thermal stability (A) Circular dichroism 200–270 nm. (B) Tertiary fingerprint CD 260–320 nm. (C) Trp fluorescence melting curves. In all parts: wild-type dashed line, P32T solid line and P32A dotted line.

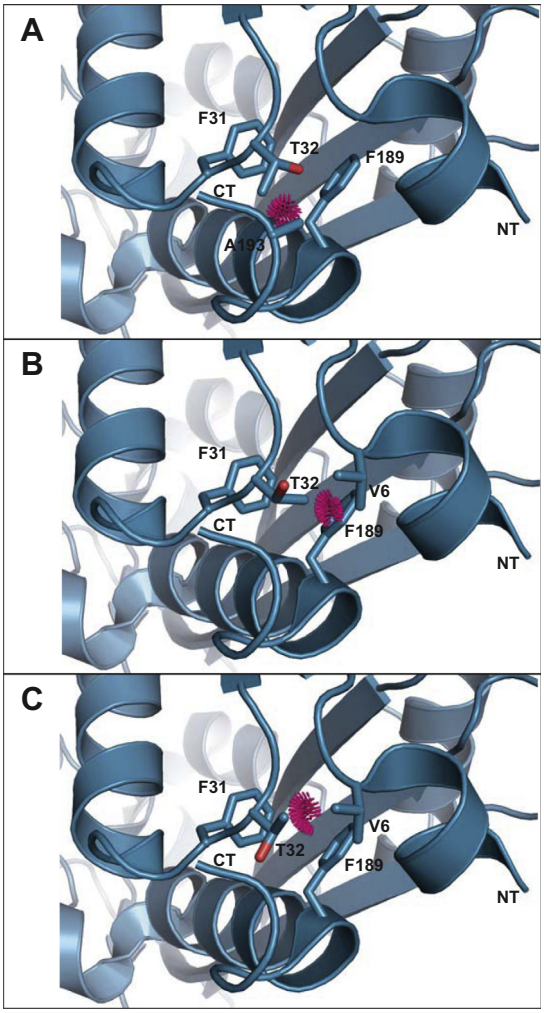

Fig.5. Steric conflicts caused by Pro32 to Thr amino acid change. (A–C) Modeling in a threonine residue for Pro32 in wild-type with three possible rotamers. In each case, a clash (red dots) of greater than 1 Å occurs with neighboring residues (Ala193 in (A); Val6 in (B) and (C)). Also, the rotamer in (A) places the polar hydroxyl group in the hydrophobic pocket containing Phe31 and Phe189. Clashes were determined with *MolProbity* (Chen et al., 2010; Davis et al., 2007) and figures were generated with *PyMOL* (Schrodinger, 2011). (For interpretation of the references to color in this figure legend, the reader is referred to the web version of this article.)

the hydrophobic surfaces of misfolded proteins, preventing aggregation and aiding in refolding (Kubota, 2009; Mayer and Bukau, 2005; Sharma et al., 2009). If this does indeed occur, then the activity in cells may be reduced due to the chaperone blocking entry into the active site. This would explain why highly purified P32T protein retains almost full ITPase activity *in vitro*.

Two other pathways could lead to proteasomal degradation. The 20S proteasome is able to directly bind partially denatured, oxidized proteins with higher surface hydrophobicity without the need for ubiquitylation (Davies and Shringarpure, 2006). Thus, the surface exposure of Phe31 may target P32T ITPA directly to the proteasome, leading to its degradation. Alternatively, the reduced stability of P32T ITPA could lead to its partial unfolding in cells, resulting in ubiquitylation and proteasomal degradation. One would expect that this would occur for P32T-wild-type heterodimers as well as for P32T homodimers, which would help explain the observed approximately 25% residual activity in 94C>A heterozygotes (Fig. 7B). This is consistent with the previously seen nearly 10-fold reduction in ITPA protein levels in fibroblasts homozygous for the 94C>A polymorphism versus wild-type fibroblasts (Stepchenkova et al., 2009). Inhibition of the proteasome, therefore, would be expected to lead to an increase in ITPA levels in P32T fibroblasts.

Now that the structure of P32T ITPA is known, it may be possible to rationally design small molecules to attempt to improve the *in vivo* activity. A small, hydrophobic molecule could potentially fit into the hole in the hydrophobic core of the protein left by Phe31. This would be expected to correct for the loss of hydrophobic interactions and improve protein stability. Such a drug could be co-administered with mercaptopurines in patients known to possess the 94C>A allele of ITPA to improve ITPA function and reduce adverse reactions.

Overall, the structure of P32T ITPA explains previous results and provides new testable hypotheses. The protein exists as a dimer

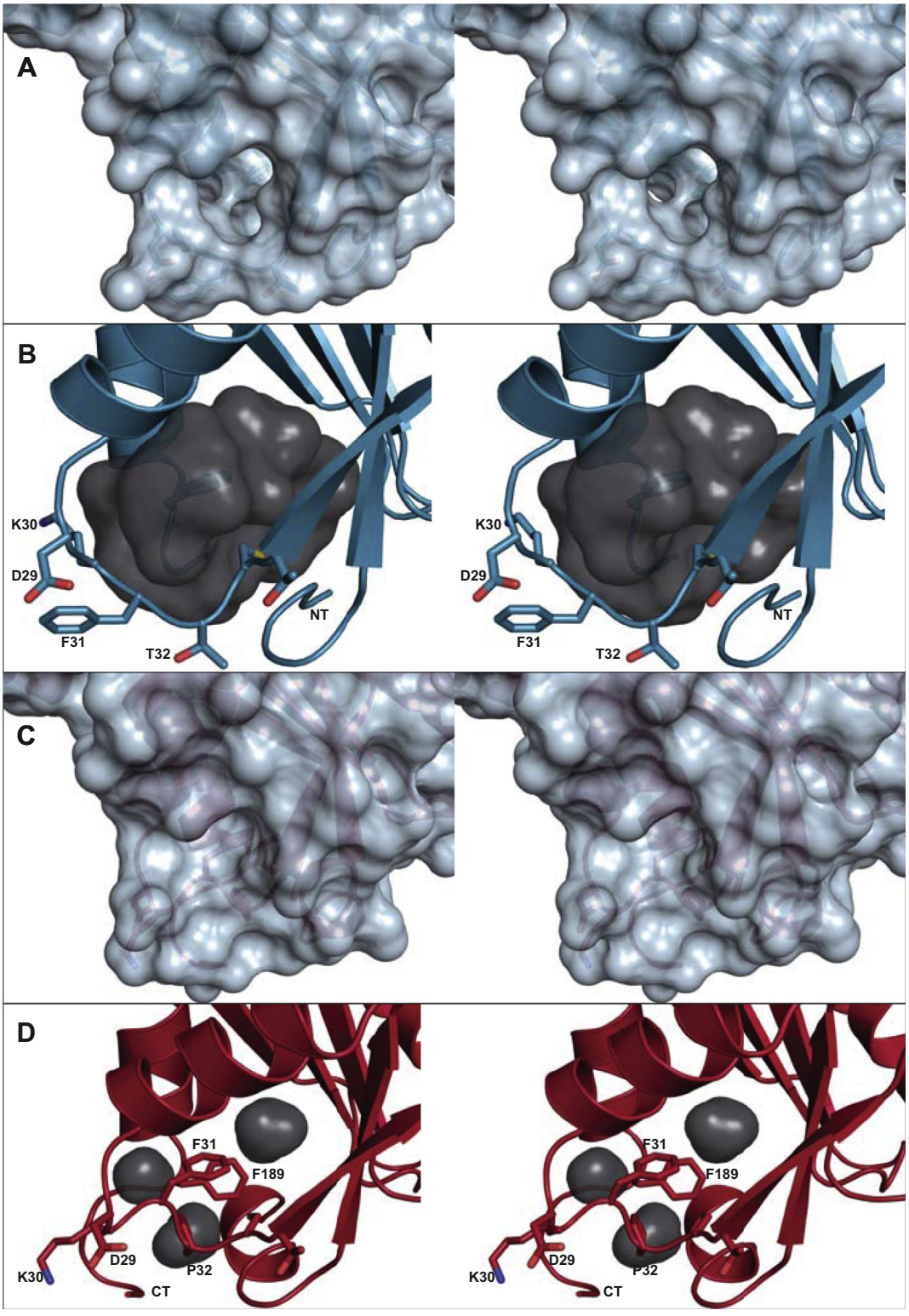

Fig.6. P32T ITPA has a hole in the hydrophobic core. (A) The solvent accessible surface (sphere radius = 1.4 Å) shows a hole in the protein structure due to Phe31 and Thr32 moving from the hydrophobic core out into the solvent. (B) An inverse view generated by *HOLLOW* (Ho and Gruswitz, 2008) demonstrating the large cavity (gray) left in the protein's core. The cavity has a volume of 887 $Å^3$ as determined by *VOIDOO* (Kleywegt and Jones, 1994). By comparison, (C) the surface of wild-type ITPA does not reveal any holes and (D) only small cavities (gray) exist in the core (volume = 159 $Å^3$). Wall-eyed stereo pairs were generated with *PyMOL* (Schrodinger, 2011).

and the lack of structural changes in the active site is consistent with the observed activity *in vitro*. The decreased thermal stability of P32T ITPA is explained by the loss of hydrophobic interactions and the concomitant exposure of Phe31 to the solvent. This exposed hydrophobic residue is likely to have other consequences, such as targeting the protein to the proteasome and binding to chaperones. Determining the extent to which these processes occur will aid our understanding of how the change of a single amino acid leads to the drastic loss of activity seen in humans.

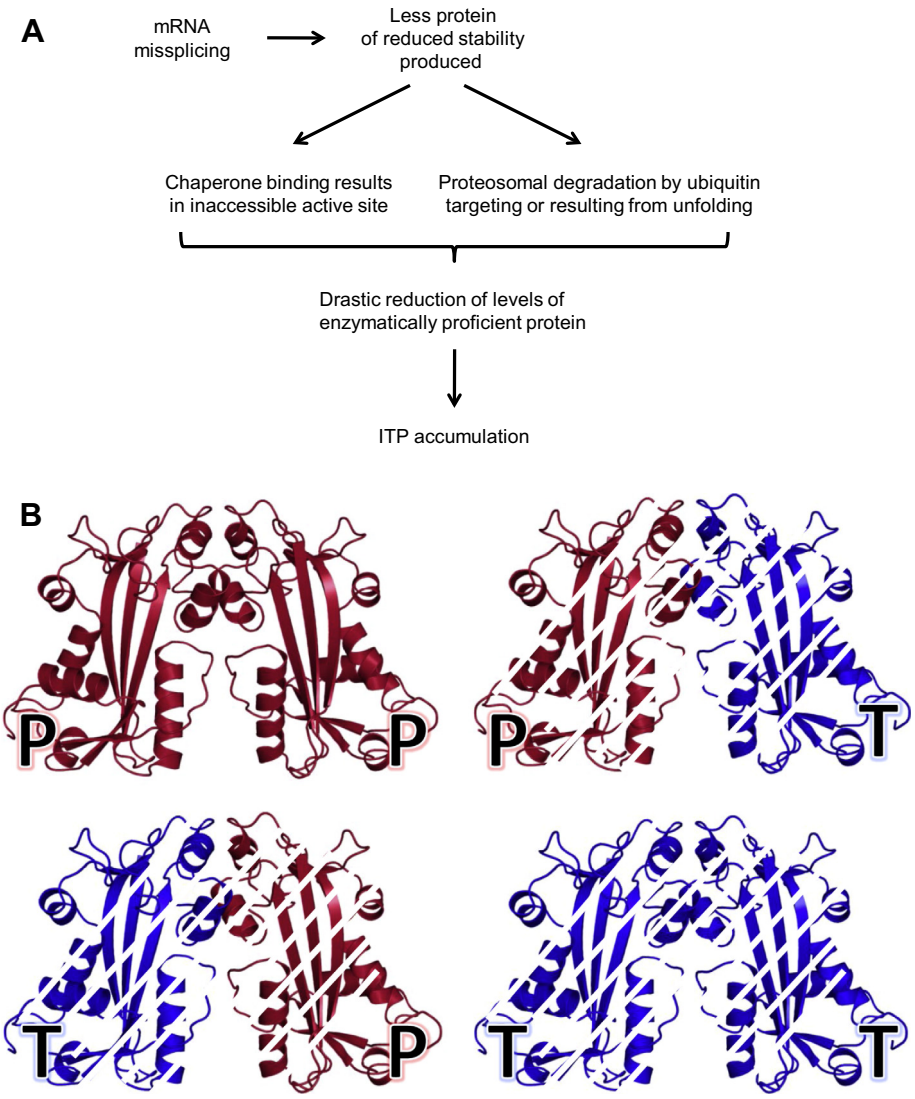

Fig.7. Models for ITPA deficiency. (A) The 94C>A polymorphism leads to an increase in the amount of mRNA that is misspliced into a non-functional variant (Arenas et al., 2007). This, in turn, leads to less protein production, and this protein is less stable. The exposed phenylalanine residue in P32T ITPA could cause chaperones to bind (left arrow) and/or target the protein to the proteasome (right arrow) for degradation. Together these would further reduce the levels of active protein levels in the cell. Ultimately, these effects culminate in a reduction in ITPA activity in the cell and therefore ITP accumulation. (B) Model explaining the dominant negative effect of the P32T change. We propose that the P32T change causes degradation of ITPA activity in both wild-type/P32T heterodimers and P32T/P32T homodimers. White hash marks indicate the degradation of dimers, as in a paper shredder (Brunger, 1993; Matthews, 1968).

5. Database accession numbers

Structure factors and atomic coordinates for the P32T mutant of ITPA have been deposited in the RCSB Protein Data Bank with accession number 4F95.

Acknowledgments

The authors would like to thank Jeff Lovelace, Jason Porta, and Carol Kolar for their technical assistance in obtaining and analyzing the X-ray diffraction data and Tahir Tahirov, Ph.D., Madeline Shea, Ph.D. and David Price, Ph.D. for their helpful discussion. We would also like to thank Hui-Ting Lee, Ph.D. for providing technical assistance in obtaining the circular dichroism data. This work was supported by the following research grants: UNMC Eppley Cancer Center seed grants (YIP and GEOB), NCI Eppley Cancer Center Support Grant P30CA036727 (GEOB), Department of Education GAANN grant P200A070554 (PDS), National Center for Research Resources grant 5P20RR016469 and the National Institute for General Medical Science grant 8P20GM103427 (GEOB and CAB); National Science Foundation grant MCB1122029 (LAM) and NCI grant CA129925, by the Russian federal program "Innovation scientific personnel" State contracts 14.740.11.0916 and the Federal Grant-in-Aid Program «Human Capital for Science and Education in Innovative Russia» (Government Contract No. 8654) (YIP).

Appendix A. Supplementary data

Supplementary data associated with this article can be found, in the online version, at http://dx.doi.org/10.1016/j.jsb.2013.03.007.

References

Abolhassani, N., Iyama, T., Tsuchimoto, D., Sakumi, K., Ohno, M., Behmanesh, M., Nakabeppu, Y., 2010. NUDT16 and ITPA play a dual protective role in maintaining chromosome stability and cell growth by eliminating dIDP/IDP and dITP/ITP from nucleotide pools in mammals. Nucleic Acids Research 38, 2891–2903.

Adams, P.D., Afonine, P.V., Bunkoczi, G., Chen, V.B., Davis, I.W., Echols, N., Headd, J.J., Hung, L.-W., Kapral, G.J., Grosse-Kunstleve, R.W., McCoy, A.J., Moriarty, N.W., Oeffner, R., Read, R.J., Richardson, D.C., Richardson, J.S., Terwilliger, T.C., Zwart, P.H., 2010. PHENIX: a comprehensive Python-based system for macromolecular structure solution. Acta Crystallographica Section D, Biological Crystallography 66, 213–221.

Andrade, M.A., Chacon, P., Merelo, J.J., Moran, F., 1993. Evaluation of secondary structure of proteins from UV circular dichroism spectra using an unsupervised learning neural network. Protein Engineering 6, 383–390.

Arenas, M., Duley, J., Sumi, S., Sanderson, J., Marinaki, A., 2007. The ITPA c.94C>A and g.IVS2+21A>C sequence variants contribute to missplicing of the ITPA gene. Biochimica et Biophysica Acta 1772, 96–102.

Behmanesh, M., Sakumi, K., Abolhassani, N., Toyokuni, S., Oka, S., Ohnishi, Y.N., Tsuchimoto, D., Nakabeppu, Y., 2009. ITPase-deficient mice show growth retardation and die before weaning. Cell Death and Differentiation 16, 1315–1322.

Bierau, J., Lindhout, M., Bakker, J.A., 2007. Pharmacogenetic significance of inosine triphosphatase. Pharmacogenomics 8, 1221–1228.

Borgstahl, G.E., 2007. How to use dynamic light scattering to improve the likelihood of growing macromolecular crystals. Methods in Molecular Biology 363, 109–129.

Brunger, A.T., 1993. Assessment of phase accuracy by cross validation: the free R value. Methods and applications. Acta Crystallographica Section D, Biological Crystallography 49, 24–36.

Burgis, N.E., Cunningham, R.P., 2007. Substrate specificity of RdgB protein, a deoxyribonucleoside triphosphate pyrophosphohydrolase. Journal of Biological Chemistry 282, 3531–3538.

Cao, H., Hegele, R.A., 2002. DNA polymorphisms in ITPA including basis of inosine triphosphatase deficiency. Journal of Human Genetics 47, 620–622.

Chen, V.B., Arendall III, W.B., Headd, J.J., Keedy, D.A., Immormino, R.M., Kapral, G.J., Murray, L.W., Richardson, J.S., Richardson, D.C., 2010. MolProbity: all-atom structure validation for macromolecular crystallography. Acta Crystallographica Section D, Biological Crystallography 66, 12–21.

Collaborative Computational Project, 1994. The CCP4 suite: programs for protein crystallography. Acta Crystallographica Section D, Biological Crystallography 50 (4), 760–763.

Davies, K.J., Shringarpure, R., 2006. Preferential degradation of oxidized proteins by the 20S proteasome may be inhibited in aging and in inflammatory neuromuscular diseases. Neurology 66, S93–S96.

Davis, I.W., Leaver-Fay, A., Chen, V.B., Block, J.N., Kapral, G.J., Wang, X., Murray, L.W., Arendall, W.B., Snoeyink, J., Richardson, J.S., Richardson, D.C., 2007. MolProbity: all-atom contacts and structure validation for proteins and nucleic acids. Nucleic Acids Research 35, W375–W383.

Emsley, P., Lohkamp, B., Scott, W.G., Cowtan, K., 2010. Features and development of Coot. Acta Crystallographica Section D, Biological Crystallography 66, 486–501.

Fellay, J., Thompson, A.J., Ge, D., Gumbs, C.E., Urban, T.J., Shianna, K.V., Little, L.D., Qiu, P., Bertelsen, A.H., Watson, M., Warner, A., Muir, A.J., Brass, C., Albrecht, J., Sulkowski, M., McHutchison, J.G., Goldstein, D.B., 2010. ITPA gene variants protect against anaemia in patients treated for chronic hepatitis C. Nature 464, 405–408.

Friedberg, E.C., Walker, G.C., Siede, W., Wood, R.D., Schultz, R.A., Ellenberger, T., 2006. DNA Repair and Mutagenesis. ASM Press.

Habel, J.E., Ohren, J.F., Borgstahl, G.E., 2001. Dynamic light-scattering analysis of full-length human RPA14/32 dimer: purification, crystallization and self-association. Acta Crystallographica Section D, Biological Crystallography 57, 254–259.

Herting, G., Barber, K., Zappala, M.R., Cunningham, R.P., Burgis, N.E., 2010. Quantitative *in vitro* and *in vivo* characterization of the human P32T mutant ITPase. Biochimica et Biophysica Acta 1802, 269–274.

Ho, B., Gruswitz, F., 2008. HOLLOW: generating accurate representations of channel and interior surfaces in molecular structures. BMC Structural Biology 8, 49.

Kabsch, W., 1976. A solution for the best rotation to relate two sets of vectors. Acta Crystallographica Section A, Foundations of Crystallography 32, 922–923.

Kadonosono, T., Chatani, E., Hayashi, R., Moriyama, H., Ueki, T., 2003. Minimization of cavity size ensures protein stability and folding: structures of Phe46-replaced bovine pancreatic RNase A. Biochemistry (Mosc.) 42, 10651–10658.

Kelly, S.M., Jess, T.J., Price, N.C., 2005. How to study proteins by circular dichroism. Biochimica et Biophysica Acta 1751, 119–139.

Kleywegt, G.J., 1997. Validation of protein models from Calpha coordinates alone. Journal of Molecular Biology 273, 371–376.

Kleywegt, G.J., Jones, T.A., 1994. Detection, delineation, measurement and display of cavities in macromolecular structures. Acta Crystallographica Section D, Biological Crystallography 50, 178–185.

Kozmin, S.G., Leroy, P., Pavlov, Y.I., Schaaper, R.M., 2008. YcbX and yiiM, two novel determinants for resistance of Escherichia coli to N-hydroxylated base analogues. Molecular Microbiology 68, 51–65.

Krissinel, E., Henrick, K., 2007. Inference of macromolecular assemblies from crystalline state. Journal of Molecular Biology 372, 774–797.

Krynetski, E.Y., Evans, W.E., 1998. Pharmacogenetics of cancer therapy: getting personal. American Journal of Human Genetics 63, 11–16.

Kubota, H., 2009. Quality control against misfolded proteins in the cytosol: a network for cell survival. Journal of Biochemistry 146, 609–616.

Lee, B., Richards, F.M., 1971. The interpretation of protein structures: estimation of static accessibility. Journal of Molecular Biology 55, 379–400.

Lin, S., McLennan, A.G., Ying, K., Wang, Z., Gu, S., Jin, H., Wu, C., Liu, W., Yuan, Y., Tang, R., Xie, Y., Mao, Y., 2001. Cloning, expression, and characterization of a human inosine triphosphate pyrophosphatase encoded by the itpa gene. The Journal of Biological Chemistry 276, 18695–18701.

Lovell, S.C., Davis, I.W., Arendall 3rd, W.B., de Bakker, P.I., Word, J.M., Prisant, M.G., Richardson, J.S., Richardson, D.C., 2003. Structure validation by Calpha geometry: phi, psi and Cbeta deviation. Proteins 50, 437–450.

Marinaki, A.M., Ansari, A., Duley, J.A., Arenas, M., Sumi, S., Lewis, C.M., Shobowale-Bakre, E.-M., Escuredo, E., Fairbanks, L.D., Sanderson, J.D., 2004. Adverse drug reactions to azathioprine therapy are associated with polymorphism in the gene encoding inosine triphosphate pyrophosphatase (ITPase). Pharmacogenetics 14, 181–187.

Marky, L.A., Breslauer, K.J., 1987. Calculating thermodynamic data for transitions of any molecularity from equilibrium melting curves. Biopolymers 26, 1601–1620.

Marsh, S., King, C.R., Ahluwalia, R., McLeod, H.L., 2004. Distribution of ITPA P32T alleles in multiple world populations. Journal of Human Genetics 49, 579–581.

Matthews, B.W., 1968. Solvent content of protein crystals. Journal of Molecular Biology 33, 491–497.

Mayer, M.P., Bukau, B., 2005. Hsp70 chaperones: cellular functions and molecular mechanism. Cellular and Molecular Life Sciences: CMLS 62, 670–684.

Menezes, M.R., Waisertreiger, I.S., Lopez-Bertoni, H., Luo, X., Pavlov, Y.I., 2012. Pivotal role of inosine triphosphate pyrophosphatase in maintaining genome stability and the prevention of apoptosis in human cells. PLoS One 7, e32313.

Ochi, H., Maekawa, T., Abe, H., Hayashida, Y., Nakano, R., Kubo, M., Tsunoda, T., Hayes, C.N., Kumada, H., Nakamura, Y., Chayama, K., 2010. ITPA polymorphism affects ribavirin-induced anemia and outcomes of therapy–a genome-wide study of Japanese HCV virus patients. Gastroenterology 139, 1190–1197.

Okada, Y., Nakamura, K., Hiromura, K., Nojima, Y., Horiuchi, R., Yamamoto, K., 2009. Pro32Thr polymorphism of inosine triphosphate pyrophosphatase gene predicts efficacy of low-dose azathioprine for patients with systemic lupus erythematosus. Clinical Pharmacology and Therapeutics 85, 527–530.

Padilla, J.E., Yeates, T.O., 2003. A statistic for local intensity differences: robustness to anisotropy and pseudo-centering and utility for detecting twinning. Acta Crystallographica Section D, Biological Crystallography 59, 1124–1130.

Pang, B., McFaline, J.L., Burgis, N.E., Dong, M., Taghizadeh, K., Sullivan, M.R., Elmquist, C.E., Cunningham, R.P., Dedon, P.C., 2012. Defects in purine nucleotide metabolism lead to substantial incorporation of xanthine and hypoxanthine into DNA and RNA. Proceedings of the National Academy of Sciences of the United States of America 109, 2319–2324.

Porta, J., Kolar, C., Kozmin, S.G., Pavlov, Y.I., Borgstahl, G.E., 2006. Structure of the orthorhombic form of human inosine triphosphate pyrophosphatase. Acta Crystallographica.Section F, Structural Biology and Crystallization Communications 62, 1076–1081.

Potterton, E., Briggs, P., Turkenburg, M., Dodson, E., 2003. A graphical user interface to the CCP4 program suite.. Acta Crystallographica Section D, Biological Crystallography 59, 1131–1137.

Relling, M.V., Hancock, M.L., Rivera, G.K., Sandlund, J.T., Ribeiro, R.C., Krynetski, E.Y., Pui, C.H., Evans, W.E., 1999. Mercaptopurine therapy intolerance and heterozygosity at the thiopurine *S*-methyltransferase gene locus. Journal of the National Cancer Institute 91, 2001–2008.

Saff, E., Kuijlaars, A., 1997. Distributing many points on a sphere. The Mathematical Intelligencer 19, 5–11.

Sakamoto, N., Tanaka, Y., Nakagawa, M., Yatsuhashi, H., Nishiguchi, S., Enomoto, N., Azuma, S., Nishimura-Sakurai, Y., Kakinuma, S., Nishida, N., Tokunaga, K., Honda, M., Ito, K., Mizokami, M., Watanabe, M., 2010. ITPA gene variant protects against anemia induced by pegylated interferon-alpha and ribavirin therapy for Japanese patients with chronic hepatitis C. Hepatology Research: The Official Journal of the Japan Society of Hepatology 40, 1063–1071.

Savitzky, A., Golay, M.J.E., 1964. Smoothing and differentiation of data by simplified least squares procedures. Analytical Chemistry 36, 1627–1639.

Schrodinger, LLC., 2011. The PyMOL Molecular Graphics System. Version 1.4.1.

Schwehm, J.M., Kristyanne, E.S., Biggers, C.C., Stites, W.E., 1998. Stability effects of increasing the hydrophobicity of solvent-exposed side chains in staphylococcal nuclease. Biochemistry 37, 6939–6948.

Sharma, S.K., Christen, P., Goloubinoff, P., 2009. Disaggregating chaperones: an unfolding story. Current Protein and Peptide Science 10, 432–446.

Shipkova, M., Franz, J., Abe, M., Klett, C., Wieland, E., Andus, T., 2011. Association between adverse effects under azathioprine therapy and inosine triphosphate pyrophosphatase activity in patients with chronic inflammatory bowel disease. Therapeutic Drug Monitoring 33, 321–328.

Stenmark, P., Kursula, P., Flodin, S., Graslund, S., Landry, R., Nordlund, P., Schuler, H., 2007. Crystal structure of human inosine triphosphatase. Substrate binding and implication of the inosine triphosphatase deficiency mutation P32T. The Journal of Biological Chemistry 282, 3182–3187.

Stepchenkova, E.I., Tarakhovskaya, E.R., Spitler, K., Frahm, C., Menezes, M.R., Simone, P.D., Kolar, C., Marky, L.A., Borgstahl, G.E., Pavlov, Y.I., 2009. Functional study of the P32T ITPA variant associated with drug sensitivity in humans. Journal of Molecular Biology 392, 602–613.

Stocco, G., Cheok, M.H., Crews, K.R., Dervieux, T., French, D., Pei, D., Yang, W., Cheng, C., Pui, C.H., Relling, M.V., Evans, W.E., 2009. Genetic polymorphism of inosine triphosphate pyrophosphatase is a determinant of mercaptopurine metabolism and toxicity during treatment for acute lymphoblastic leukemia. Clinical Pharmacology and Therapeutics 85, 164–172.

Strub, C., Alies, C., Lougarre, A., Ladurantie, C., Czaplicki, J., Fournier, D., 2004. Mutation of exposed hydrophobic amino acids to arginine to increase protein stability. BMC Biochemistry 5, 9.

Sumi, S., Marinaki, A.M., Arenas, M., Fairbanks, L., Shobowale-Bakre, M., Rees, D.C., Thein, S.L., Ansari, A., Sanderson, J., De Abreu, R.A., Simmonds, H.A., Duley, J.A.,

2002. Genetic basis of inosine triphosphate pyrophosphohydrolase deficiency. Human Genetics 111, 360–367.
Thompson, A.J., Fellay, J., Patel, K., Tillmann, H.L., Naggie, S., Ge, D., Urban, T.J., Shianna, K.V., Muir, A.J., Fried, M.W., Afdhal, N.H., Goldstein, D.B., McHutchison, J.G., 2010. Variants in the ITPA gene protect against ribavirin-induced hemolytic anemia and decrease the need for ribavirin dose reduction. Gastroenterology 139, 1181–1189.
Verhoef, V.L., Fuller, S.A., Morris, A.J., 1980. Individual variation of nucleoside triphosphate pyrophosphohydrolase activity in human erythrocytes, granulocytes, lymphocytes, and platelets. Biochemical Genetics 18, 235–245.
Vogel, H.J., Bonner, D.M., 1956. Acetylornithinase of Escherichia coli: partial purification and some properties. Journal of Biological Chemistry 218, 97–106.
Waisertreiger, I.S., Menezes, M.R., Randazzo, J., Pavlov, Y.I., 2010. Elevated levels of DNA strand breaks induced by a base analog in the human cell line with the P32T ITPA variant. Journal of Nucleic Acids 2010, 11 [2010/10/12 ed.].
Whitmore, L., Wallace, B.A., 2004. DICHROWEB, an online server for protein secondary structure analyses from circular dichroism spectroscopic data. Nucleic Acids Research 32, W668–W673.
Yeates, T.O., 1997. Detecting and overcoming crystal twinning. Methods in Enzymology 276, 344–358.

SUPPLEMENT

The human ITPA polymorphic variant P32T is destabilized by the unpacking of the hydrophobic core

Peter D. Simone, Lucas R. Struble, Admir Kellezi, Carrie A. Brown, Corinn E. Grabow, Irine Khutsishvili, Luis A. Marky, Youri I. Pavlov, and Gloria E.O. Borgstahl

Supplemental Figure

Figure S1. Structural highlights of ITPA (A) Dimer interface of P32T ITPA. The dimer interface of P32T ITPA is shown as a cartoon representation with residues in the interface shown as sticks. Residues are colored as follows: glutamic acid = green, glutamine = magenta, leucine = brown, lysine = gray, phenylalanine = red, tryptophan = orange, tyrosine = dark blue. Many hydrophobic interactions are readily apparent. The interface also contains several hydrogen bonds involving hydrophilic residues and the peptide backbone. This interface buries approximately 1100 $Å^2$ of surface area. Positions of aromatic residues for (b) wild-type ITPA and (C) P32T ITPA (Trp are green, Tyr are orange and Phe are blue).

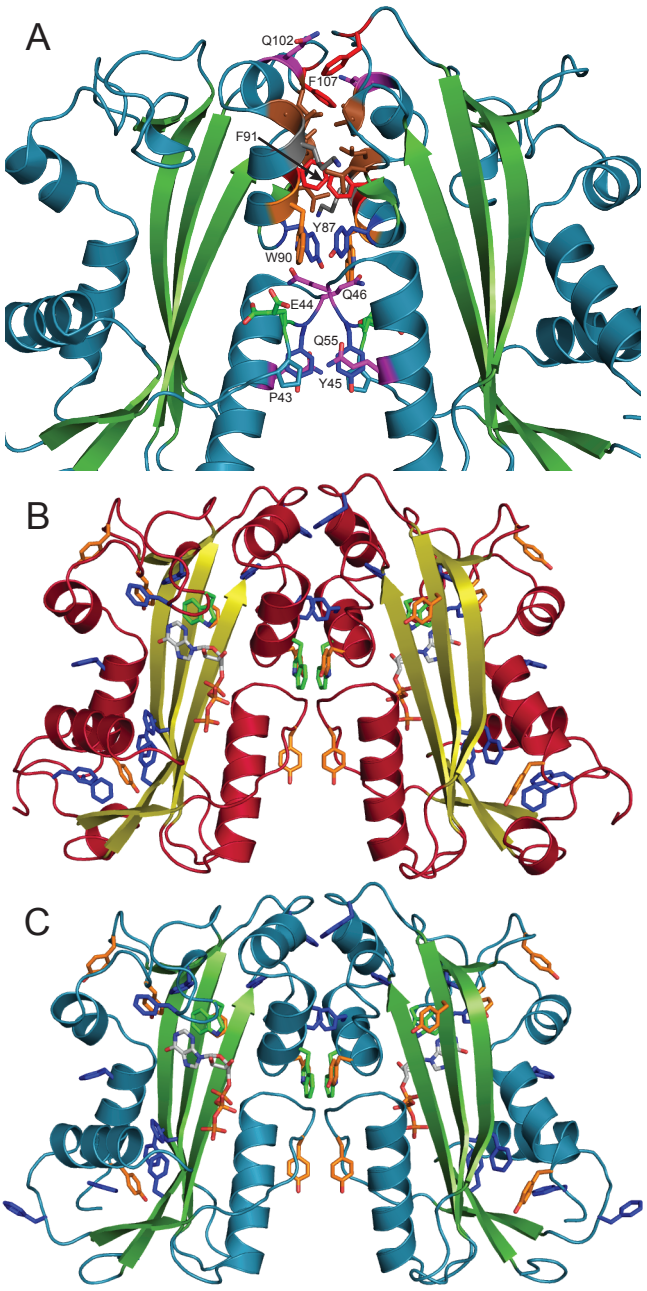
A
Q102
F107
F91
Y87
W90
E44
Q46
Q55
P43
Y45
B
C